Barotropic Vortex Evolution on a Beta Plane

LLOYD J. SHAPIRO AND KATSUYUKI V. OOYAMA

Hurricane Research Division/AOML, Miami, Florida

(Manuscript received 13 April 1989, in final form 17 August 1989)

ABSTRACT

A barotropic, primitive equation (shallow water) model is used on the beta plane to investigate the influence of divergence, total relative angular momentum (RAM) and advective nonlinearities on the evolution of a hurricane-like vortex. The multinested numerical model is based on the spectral application of a finite element representation. The undisturbed fluid depth is taken to be 1 km. Scaling of the vorticity equation, in conjunction with a Bessel function spectral decomposition, indicates that divergence should have a very small effect on the hurricane motion. Simulations with an initially symmetric cyclonic vortex in a resting environment confirm this analysis, and contradict previous published studies on the effect of divergence in a barotropic model.

During a 120 h simulation the cyclonic vortex develops asymmetries that have an influence far from the initial circulation. The total RAM within a large circle centered on the vortex decreases with time, and then oscillates about zero. For circles with radii $\leq$ 1000 km, the total RAM approaches, but does not reach, zero. An angular momentum budget indicates that the horizontal angular momentum flux tends to counteract the net Coriolis torque on the vortex. If the total RAM of the initial symmetric vortex is zero, the weak far-field asymmetries are essentially eliminated. The motion of the vortex is not, however, related to the RAM in any simple way.

Within a few days the near-vortex asymmetries reach a near-steady state. The Asymmetric Absolute Vorticity (AAV) is nearly uniform within ~350 km of the vortex center. The homogenization of AAV, which occurs within the closed vortex gyre, is likely due to shearing by the symmetric wind, combined with removal of energy at the smallest scales. The homogenization effectively neutralizes the planetary beta effect, as well as the vorticity associated with an environmental wind.

1. Introduction

A tropical cyclone is a particularly persistent, coherent atmospheric system that may last for many days. Its symmetric azimuthal wind is in near-gradient balance over the bulk of the cyclone vortex (Willoughby 1989). Neglect of the convectively driven secondary circulation that maintains the azimuthal wind allows the idealization of the cyclone as a nearly steady, axisymmetric, free-spinning vortex. Even in the absence of dissipation, and in a quiescent environment, such a vortex cannot, however, remain strictly steady. Advection of planetary vorticity leads to the development of asymmetries that distort and displace the vortex. The partitioning between distortion and displacement has been the subject of theoretical study (Kasahara and Platzman 1963; Willoughby 1988). Without convection to maintain it, a barotropic vortex is eventually destroyed by Rossby wave dispersion (McWilliams and Flierl 1979). The relative success of barotropic numerical models in forecasting hurricane tracks over several days (e.g., Neumann and Pelissier 1981; Goldenberg et al. 1987; DeMaria 1987) is testimony, however, to the persistence of the model vortex on synoptic time scales.

A nondivergent barotropic model is the simplest system that contains the essential physics of vortex motion. Prognostic numerical experiments with such a model (e.g., DeMaria 1985; Chan and Williams 1987; Fiorino and Elsberry 1989a) indicate that an initially symmetric hurricane-like vortex on a beta plane moves to the northwest. After a day or two of adjustment, a near-uniform motion is established with a speed of several meters per second. The circulation about the vortex center develops asymmetries that both distort the vortex and provide the current that advects the vortex center. The symmetric circulation evolves as well.

The influence of the extremely high inertial stability of the hurricane core, though implicit in the specification of the free-spinning vortex, is not included in a nondivergent model. A barotropic, primitive equation (shallow water) model allows divergence to play a role, while excluding explicit physical processes such as cumulus convection and boundary layer dissipation that maintain the meridional circulation. Inertial effects can

Corresponding author address: Dr. Lloyd Shapiro, NOAA/AOML/HRD, 4301 Rickenbacker Causeway, Miami, FL 33149.

then alter the evolution of the vortex through vortex-tube stretching. Section 2 describes the barotropic numerical model used in the present study. Anthes and Hoke (1975), using both a shallow water and a nondivergent model, inferred that divergence has a large effect on vortex motion. The effect of divergence on the evolution of an initially symmetric hurricane-like vortex is evaluated in section 3 with a shallow water model, and the conclusion of Anthes and Hoke (1975) is reevaluated from a comparison with a nondivergent simulation.

The importance of the total relative angular momentum (RAM) of a vortex in its subsequent evolution has been recognized since Rossby (1948) attributed the northward drift of a cyclonic vortex to a net northward Coriolis force proportional to its RAM. As proven by Flierl et al. (1983), an isolated vortex on the beta plane will not remain isolated unless its net RAM is zero. Rossby's net northward force is accompanied by changes in the net RAM. Fiorino and Elsberry (1989a) show that an initially cyclonic symmetric vortex develops an outer anticyclone that tends to decrease the total RAM inside a 2000 km radius. The evolution of the RAM of an initially symmetric vortex, and the processes that determine it, are evaluated in section 4. Both an initially cyclonic vortex and one with zero total RAM are considered.

An alternate perspective on the northward vortex drift was given by Ooyama (1984). He noted that vortex motion is governed by the advective interaction among different spectral components. The small-scale components, which define the vortex center, are relatively unaffected by the beta effect. Larger-scale components, which comprise the outer vortex, move more rapidly to the west due to Rossby wave dispersion. The large-scale components then advect the small-scale components to the north. This multiscale interaction was one of the motivating factors for the development of the multinested numerical model described in section 2. Chan and Williams (1987), and Fiorino and Elsberry (1989a,b) discuss further implications of the multiscale interactions.

As the motion of the vortex becomes nearly uniform, the asymmetries near the vortex core appear to evolve to a nearly steady state as well. Fiorino and Elsberry (1989a) illustrate the establishment of the quasi-steady large-scale gyres that advect the vortex to the northwest. The characteristics of the quasi-steady state, and the mechanism that allows it to be established without severe distortion of the symmetric vortex, are evaluated in section 5.

The study by Kasahara and Platzman (1963) indicated that a background current would accelerate the vortex in the direction of the current's vorticity gradient. DeMaria's (1985) numerical experiments confirmed this result. Section 6 evaluates the influence of a background vorticity gradient on the evolution of the vortex.

2. Barotropic model; benchmark experiment

The shallow water equations, used in the bulk of the present paper, are

$$D\mathbf{u}/Dt + f\mathbf{k} \times \mathbf{u} = -\nabla\phi \tag{1}$$

$$D\phi/Dt + \phi\delta = 0, \tag{2}$$

where $\mathbf{u} = (u, v)$ is the horizontal velocity, $\delta = \nabla \cdot \mathbf{u}$, ϕ is the geopotential, f is the Coriolis parameter, and the total rate of change $D\{\ \}/Dt = (\partial/\partial t + \mathbf{u}\cdot\nabla)\{\ \}$. Here $\phi = gh$, where g is the acceleration of gravity and h the fluid depth; $f = f_0 + \beta y$, where the constants f_0 and β represent f and its northward gradient at the central latitude $\theta_0 = 20°$N.

The undisturbed fluid depth is taken to be $h = 1$ km, corresponding to the equivalent depth of an internal vertical mode with phase speed $(gh)^{1/2} = 99$ m s^{-1}. It is recognized that the atmosphere has no lid and thus, unlike the oceanic case, no free (unforced) internal modes (Lindzen 1967). Lindzen and Nigam (1987) criticize Gill's (1980) model of heat-induced tropical circulations in this context. Internal heating due to cumulus convection does, however, project primarily onto internal modes with equivalent depth less than 1 km (Lim and Chang 1983). The use of a single vertical mode in the shallow water formulation allows some representation of divergent effects and adjustments due to internal processes. Vertical modal coupling that is present in a baroclinic model is, however, completely excluded. Anthes and Hoke (1975) used a shallow water depth of 5 km to simulate the effect of vertically averaged divergence on hurricane motion. Similarly, Kitade (1981) used a depth of 3 km in his vortex motion study. The undisturbed depth $h = 1$ km in the present paper increases the potential effect of divergence over that of Anthes' or Kitade's simulation.

The numerical method used to solve the coupled system (1) and (2) is based on the Spectral Application of a Finite Element Representation (SAFER). The essence of the SAFER method is described in Ooyama (1984). The model is multinested, with each variable (u, v, and h) represented as a cubic B-spline on each subdomain [see the Appendix of Ooyama (1987)]. The splines are continuous up to the second derivative. The spline amplitudes are represented on equally spaced nodes within each subdomain. The use of the continuous, differentiable representation drastically reduces the wave phase speed errors present in discrete grid-point methods. For the experiments in the present paper the full model domain is a 15 360 km square. The model uses seven nested square meshes; the innermost is 240 km square with $\Delta = 10$ km nodal spacing. The nodal spacing Δ increases by a factor of 2 for each successively larger mesh. Interface conditions between the meshes retain continuity of the second derivative. The meshes are designed to move automatically so as to keep the model vortex as close as possible to the center of each mesh.

Wavelengths less than 2Δ, for each subdomain, are not represented in the numerical model. A derivative constraint is applied to the spline representation, acting as a sixth-order low-pass filter on the variables [Appendix of Ooyama (1987)]. The filter wavelength is essentially proportional to the distance from the vortex center, and is designed to remove effectively wavelengths less than $\sim 4\Delta$ at the outer edge of each subdomain. When information passes across the interface onto a coarser mesh, such wavelengths cannot be represented. The cubic B-spline representation allows considerable flexibility in the choice of boundary conditions. The outer boundary condition in the present study is "open," except as noted in section 6, with the second derivative normal to the boundary set equal to zero for each variable. To avoid a slow drift of the variables at scales greater than the extent of the full domain, the outer boundary values are relaxed back towards the initial condition. The outer boundary condition is thus, in effect, between open and fixed. Time differencing of the equations is leapfrog, with time step $\Delta t = 22.5$ s on the innermost mesh.

The vortices used in the model simulations are initially symmetric, with maximum tangential wind $V = 40$ m s^{-1} at a radius $r = 40$ km from the center. The vortex and meshes are initially centered at $\theta_0 = 20°$. The wind profiles $V(r)$, shown in Fig. 1, are based on the specification in appendix C of Willoughby (1988). Outside the radius of maximum wind the profile is a cubic polynomial, with $V = 0$ at $r = 1000$ km. The depth $h(r)$ is in symmetric gradient balance with the wind, with the Coriolis parameter taken as the constant f_0. At the vortex center $h = 600$ m, with corresponding phase speed $(gh)^{1/2} = 77$ m s^{-1}. The total vortex RAM is given by

$$\text{RAM} = \iint (hrV)dA, \qquad (3)$$

where the areal integral is over the region where $V \neq 0$. The vortex given by the solid line in Fig. 1 is cyclonic throughout; that given by the dashed line has an outer anticyclone of sufficient strength that RAM = 0.

The benchmark experiment of this paper is for the initially cyclonic vortex in a quiescent environment. Figure 2 displays the wind field for this experiment *after a* 120 h integration of the shallow water model. To give a complete perspective on the model solution, each of the seven submeshes is displayed.

The nondivergent simulation made in section 3 is based on the nondivergent barotropic vorticity equation on a β-plane. The prognostic variable is vorticity (ζ), with the streamfunction (ψ) derived from the elliptic equation $\nabla^2\psi = \zeta$. The model formulation is identical to that for the shallow water model, except for the outer boundary condition, which is taken to be $\psi = 0$.

3. Effect of divergence

Anthes and Hoke (1975) made nondivergent and shallow water experiments in a 2400 km square domain. The initial tangential wind in their divergent shallow water model was asymmetric, in gradient balance with a specified symmetric height field. The initial tangential wind in the nondivergent model was symmetric, in gradient balance with the same symmetric height, but with the Coriolis parameter taken as the constant f_0. Both initial vortices were very broad, with a maximum tangential wind $V \sim 30$ m s^{-1} at $r \sim 240$ km, but had $V = 0$ outside $r = 600$ km. By 48 h the vortex in the divergent model was about 50 km west and 350 km north of its initial position, while that in the nondivergent model was about 50 km further to the north and 150 km further to the west [see Fig. 1 of Anthes and Hoke (1975)]. The authors attributed the substantially slower westward motion of the vortex in the divergent model to an effect similar to the well-known Rossby wave speed reduction due to divergence.

Anthes and Hoke (1975) also explicitly estimated the magnitude of the divergent effect in the vicinity of the anticyclone that developed to the east of the vortex. The corresponding anticyclone in the benchmark experiment appears in Fig. 2 with a magnitude ~ 5 m s^{-1}. Anthes and Hoke (1975) found that ". . . for a

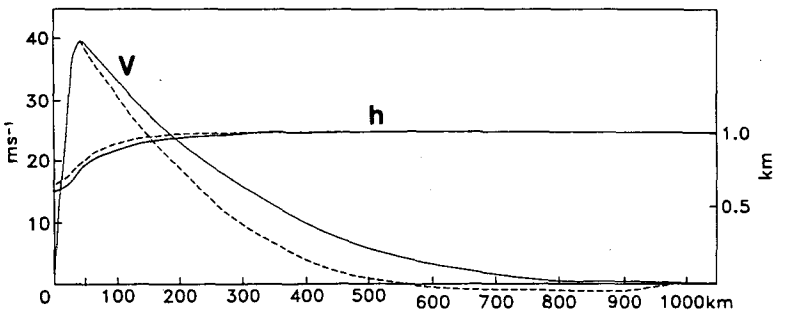

FIG. 1. Initial symmetric tangential winds $V(r)$, and heights $h(r)$ in symmetric gradient balance with V at 20°N. Solid lines are for cyclonic vortex, dashed lines for vortex with total RAM = 0.

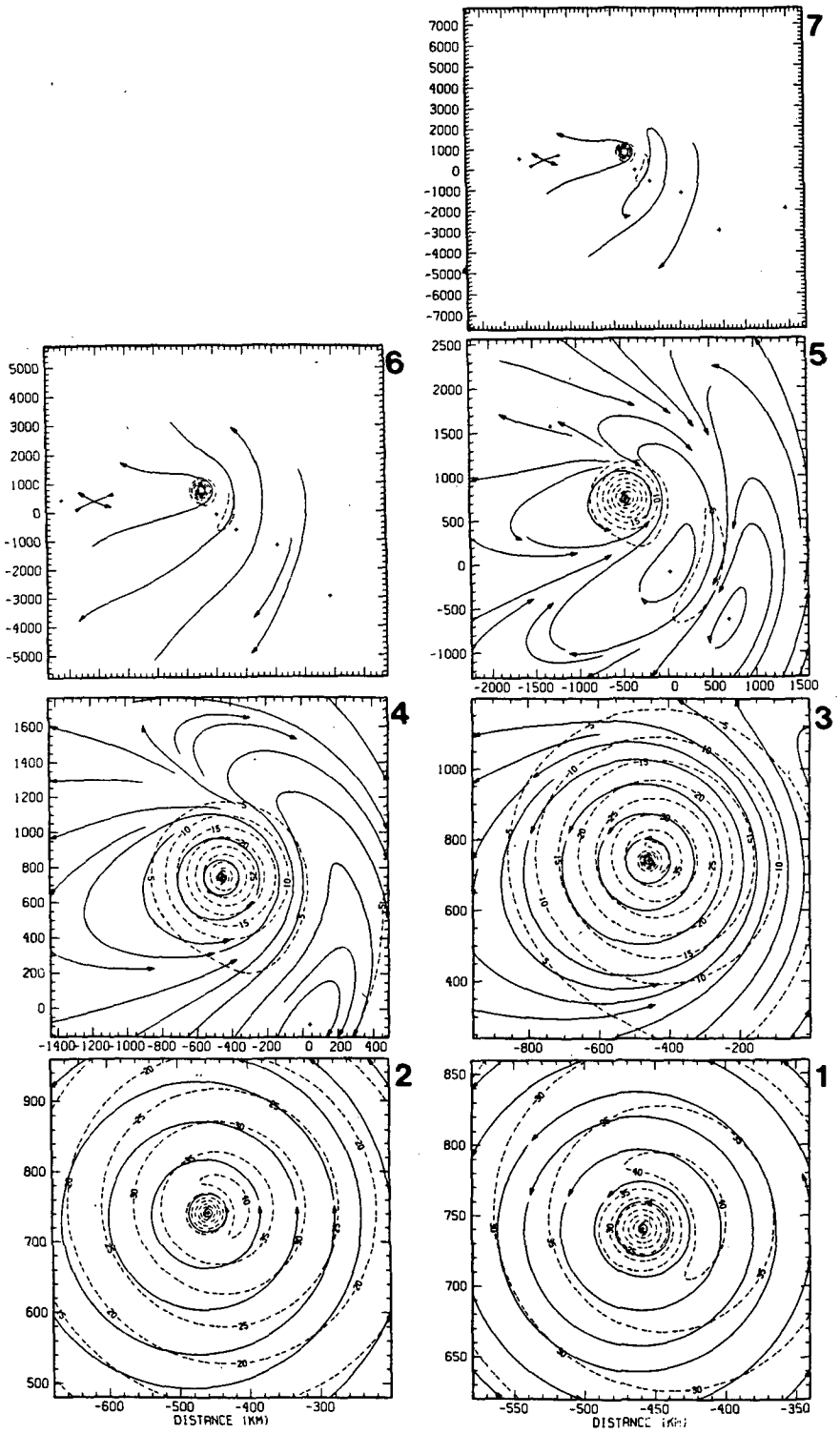

FIG. 2. Winds at 120 h for benchmark experiment, with initial cyclonic vortex. Each of the seven submeshes is numbered. Isotach interval is 5 m s^{-1}.

mean depth of 5 km, the change in absolute vorticity due to convergence is negligible compared to the change in relative vorticity due to the beta effect, and the strength of the nondivergent and divergent anticyclones is nearly the same." Since the establishment of the anticyclone is associated with the development

of the large-scale gyres that move the vortex (Fiorino and Elsberry 1989a), it is difficult to reconcile this result with the substantial differences found between the vortex displacements in the two models, unless these differences were not due to the effect of divergence.

An a priori estimate of the magnitude of the divergent influence on vortex evolution in a barotropic model can be made from a scale analysis of the vorticity equation

$$D\zeta/Dt + \beta v + (f + \zeta)\delta = 0, \tag{4}$$

derived from the curl of (1). The scaling $t \sim (\beta L)^{-1}$ in (4), where L is the horizontal length scale, applies to a vortex whose evolution is controlled primarily by planetary dispersive effects (cf. McWilliams and Flierl 1979). With a velocity scale V^*, vorticity ζ^*, $\nabla \sim 1/L$, and a vortex in near-gradient balance, (2) implies

$$\begin{aligned}(f + \zeta)\delta &= -[(f + \zeta)/h]Dh/Dt \\ &\sim [(f + \zeta^*)/h]\beta L^2(fV^* + V^{*2}/L)/g \\ &= [(f + \zeta^*)(f + V^*/L)(L^2)/(gh)]\beta V^*.\end{aligned}$$

The relative contribution of divergent and dispersive effects, $(f + \zeta)\delta/(\beta V)$, is thus measured by the parameter

$$\begin{aligned}\gamma'^2 &= (f + \zeta^*)(f + V^*/L)(L^2)/(gh) \\ &\equiv (L/R')^2.\end{aligned}$$

Here $R' = (gh/[(f + \zeta^*)(f + V^*/L)])^{1/2}$ is a local Rossby radius of deformation, where $(f + \zeta^*)(f + V^*/L)$ is the generalization of f^2 to a gradient vortex. When R' is much larger than the scale of the vortex, as in a very deep fluid (large h), divergence has a very small effect on the vortex evolution.

The vortices used by Anthes and Hoke (1975) are characterized by $V^* \sim 30$ m s^{-1}, $L \sim 240$ km, $\zeta^* \sim V^*/L \sim 10^{-4}$ s^{-1}, and $h = 5$ km. With the vortex near 20°N, $\gamma'^2 = 0.01$ and $R' = 1980$ km. Thus, divergence should have had little effect on vortex evolution and motion in Anthes and Hoke's (1975) simulation. The only possible way that divergent effects could have been important is if the vortex had substantial energy at very large scales. Then, if $L \sim R' \sim (gh)^{1/2}/f \sim 4500$ km, divergent effects could substantially alter the vortex evolution. Since the entire vortex is initially contained inside $r = 600$ km, however, scales $L \sim 4500$ km are essentially absent. One can only conclude that the differences between the divergent and nondivergent simulations up to ~48 h in Anthes and Hoke (1975) are primarily due to the differences between the initial conditions of the models. The symmetric vortex in the nondivergent model moved to the northwest, as expected from more recent modeling results (see section 1). The asymmetric vortex in the divergent model apparently moved in a more northerly direction because of a net westerly flow across the vortex evident in the initial conditions outside $r = 240$ km [see Fig. 3 of Anthes and Hoke (1975)]. The interactions between the vortices and the model domain boundaries may also contribute to differences after ~48 h.

For the vortices in Fig. 1, the vortex core is characterized by $V^* \sim 40$ m s^{-1}, $L \sim 40$ km, and $\zeta^* \sim 2V^*/L \sim 2 \times 10^{-3}$ s^{-1}. At such a small scale, the influence of β on the vortex is very small. Nevertheless, with $h = 1$ km, $\gamma'^2 = 0.33$ and $R' = 70$ km. Thus, divergence may have an influence on the inner vortex core comparable to that of the β-effect. The effect of divergence on vortex motion depends, however, on the spectrum of scales present. The natural basis functions for a spectral decomposition of a symmetric vortex are Bessel functions (cf. Flierl 1977). We decompose the angular momentum of the vortex by defining

$$sH(s) = -\int [rV(r)J_1(sr)r]dr, \tag{5}$$

where J_1 is the order-one Bessel function of the first kind. The small contribution from variations in h have been omitted for simplicity, and $H(s)$ defines the spectral amplitude at scale $1/s$. Use of the Fourier–Bessel inversion formula then gives

$$\int [(rV)^2 r]dr = \int H^2 s^4 d[\ln(s)], \tag{6}$$

where the limits of integration in both integrals are $[0, \infty]$. The spectrum H^2s^4 represents the squared angular momentum (analogous to energy) contained in the scale increment $d[\ln(s)]$. Zangvil (1977) demonstrates the advantages of a log presentation for defining a dominant scale.

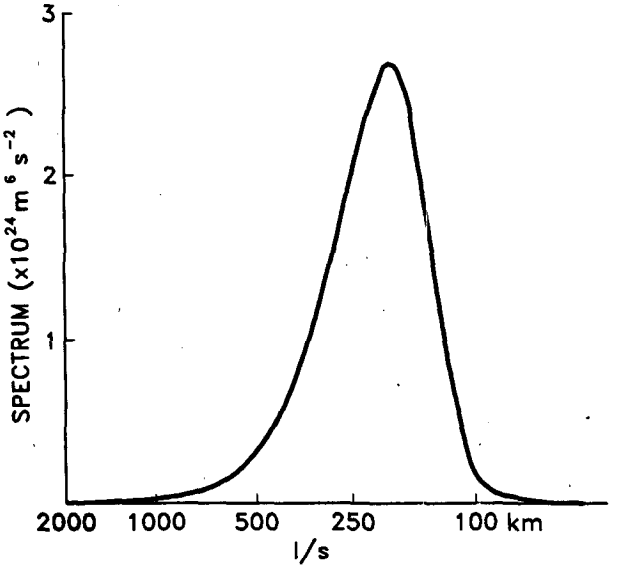

FIG. 3. Spectrum of squared angular momentum for the symmetric cyclonic vortex used in the benchmark experiment. Abscissa is given on a log scale.

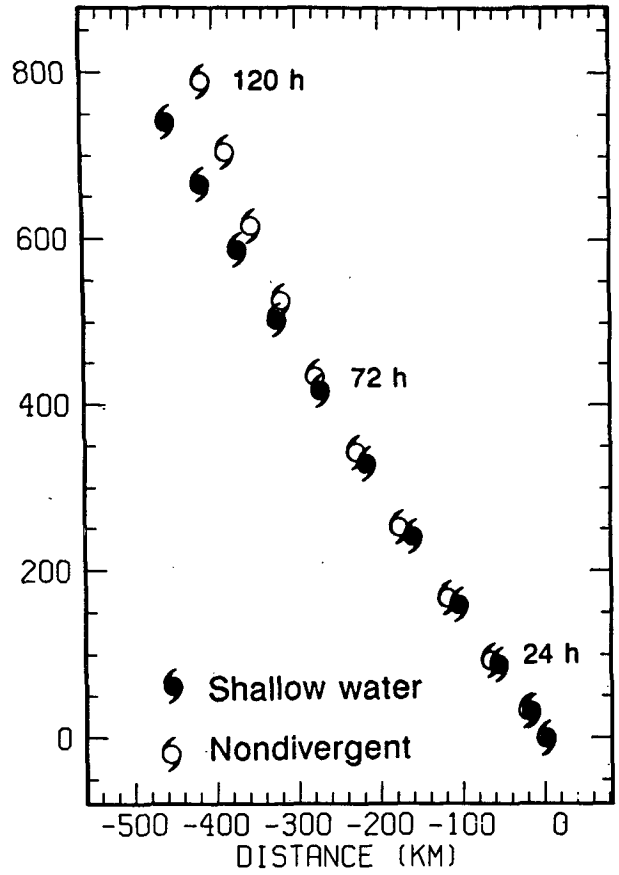

FIG. 4. Positions of vortex center every 12 h for benchmark experiment with cyclonic vortex in shallow water and nondivergent models.

Figure 3 shows the spectrum of squared angular momentum for the cyclonic vortex in Fig. 1. The dominant peak is centered at the scale $1/s \sim 200$ km. There is very little contribution to the squared angular momentum from either the vortex core scale $1/s < 100$ km, or near the scale of the planetary Rossby radius of deformation, $(gh)^{1/2}/f \sim 2000$ km. The dominant spatial scale is much smaller than the planetary Rossby radius of deformation. Since $\nabla^2[J_1(sr)] = -(s^2 - 1/r^2)J_1(sr)$, for large r the scale $1/s$ is equivalent to L used above in scaling the vorticity equation. By this scale analysis, divergence should have a very small effect on vortex motion. The absence of scales $\leqslant 100$ km, which correspond to wavelengths $\leqslant 600$ km, explains why changes in the wind profile in the inner region of a cyclone vortex, within ~300 km of the vortex center, have little effect on motion (DeMaria 1985; Fiorino and Elsberry 1989a). The dominant scale of 200 km corresponds to a wavelength ~ 1200 km. Fiorino and Elsberry (1989b) term this wavelength "medium scale." Their use of streamfunction in their two-dimensional Fourier decomposition of a symmetric cyclone vortex, and their use of a log–log plot that is not area preserving, emphasize larger scales than those evident in Fig. 3.

Divergence effects on barotropic vortex motion can be explicitly evaluated from model simulations. Figure 4 shows the vortex track in the benchmark experiment (Fig. 2), with the shallow water model ($h = 1$ km), as well as that in an experiment with the nondivergent model described at the end of section 2. The initial wind fields in the two model experiments are identical. The vortex center in the nondivergent model is defined by the vorticity maximum. In the divergent model it is defined by the height minimum, which virtually coincides with the vorticity maximum. Divergence is seen to have a very small effect on the cyclone's motion. After 72 h there is only a 21 km vector difference in net displacement (out of a 510 km total) between the nondivergent and divergent model simulations. After 120 h there is only a 71 km difference (out of a 930 km total). For a shallow water depth of 4 km, the differences between the nondivergent and divergent model simulations are even smaller (not shown). These results confirm the scale analysis above, and so contradict the inference of Anthes and Hoke (1975).

It was noted above that divergence could play a role in the evolution of the inner vortex core. Figure 5 displays the divergence quadrapole that is centered on the radius of maximum wind in the benchmark experiment. A similar quadrapole is shown in Fig. 17 of McWilliams et al. (1986) for the interface vertical velocity in a two-layer model of an evolving balanced vortex on the β-plane. Since the hurricane-like vortex in the present experiment has a much higher Rossby

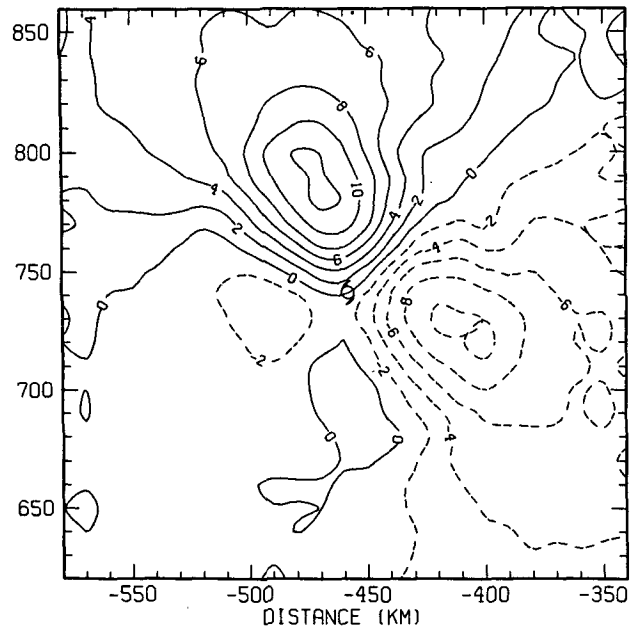

FIG. 5. Divergence ($\times 10^{-7}$ s^{-1}) for benchmark experiment at 120 h.

number than does their oceanic case, the present quadrupole is much better defined. The magnitude of the quadrupole is, however, very weak. The maximum $\delta \sim 10^{-6}$ s^{-1} is only 0.1% of the maximum $\zeta \sim 10^{-3}$ s^{-1} (not shown) in the same region. In agreement with the scale analysis above, vortex stretching $(f + \zeta)\delta \sim 10^{-9}$ s^{-2} has about the same contribution to the vorticity evolution in the vortex core as does $\beta V \sim 10^{-9}$ s^{-2}. The time scale for changes in vorticity due to stretching is $\zeta/[(f + \zeta)\delta] \sim 10$ days. Modifications to the structure of the inner core due to the divergence quadrupole are slow.

4. Influence and evolution of RAM

a. Benchmark vortex

The cyclonic vortex in the benchmark experiment develops asymmetries that have an influence far from the initial circulation (Fig. 2). The remote influence of the evolving vortex is seen even more strikingly in Fig. 6a, where the isotach interval is taken as 0.1 m s^{-1}. A strong asymmetric gyre appears to the east of the cyclone center. The corresponding feature in Anthes and Hoke's (1975) model was discussed in section 3. A series of alternating cyclonic/anticyclonic gyres extends far to the southeast behind the primary vortex.

The cause of the remote perturbations can be inferred directly from RAM considerations. Under conditions relevant to barotropic models, Flierl et al. (1983) prove that, ". . . any *slowly varying* (not necessarily uniformly propagating) and *isolated* disturbance on the beta plane must have zero net angular momentum. . . ." The theorem is independent of the presence of a background flow, if any. Strictly speaking, an isolated disturbance is one with velocity $v = o(1/r^3)$ so that the total RAM is finite. A disturbance is slowly varying if $v_t = o(1/r^3)$ as well, so that it remains isolated (at least for short times). If the initial vortex has RAM $\neq 0$, it cannot remain isolated. The system adjusts by radiating Rossby waves. The strength of the remote radiation field is proportional to the initial RAM.

The initial cyclonic vortex in the numerical experiments is confined within a finite radius and is thus isolated. Since the initial RAM $\neq 0$, however, it does not remain isolated. The gyres far to the east of the vortex in Fig. 6a, as well as the asymmetries far to the west, comprise the remote Rossby radiation field. The gyres to the east are generated by Rossby waves with scales (wavelength/2π) much less than the Rossby radius of deformation (~2000 km) and thus eastward group velocity. These perturbations, though weak, can make a substantial contribution to the RAM about the vortex center. Therefore, the RAM depends on the region over which it is computed.

The natural coordinate system for evaluating changes in vortex structure and RAM is one that trans-

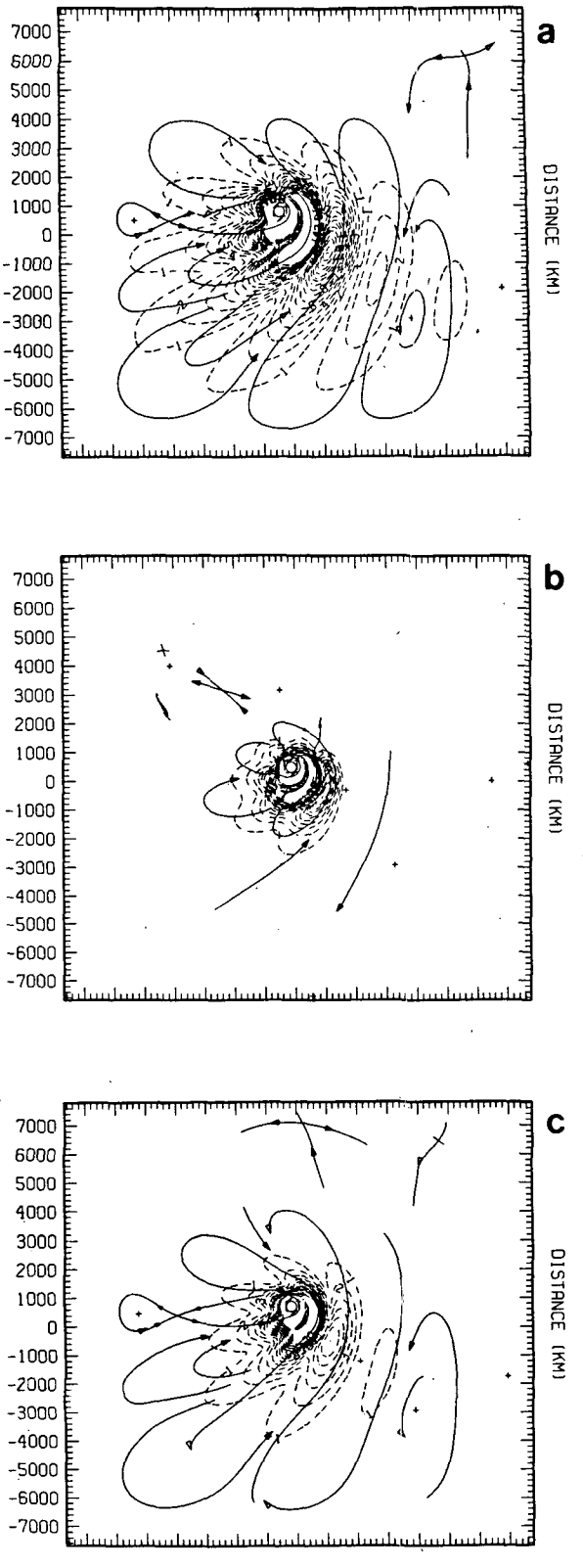

FIG. 6. Wind at 120 h for vortex with initially (a) cyclonic winds (benchmark experiment), (b) total RAM = 0, and (c) intermediate RAM (see text). Isotach interval is 0.1 m s^{-1}, and only winds ≤ 2 m s^{-1} are shown.

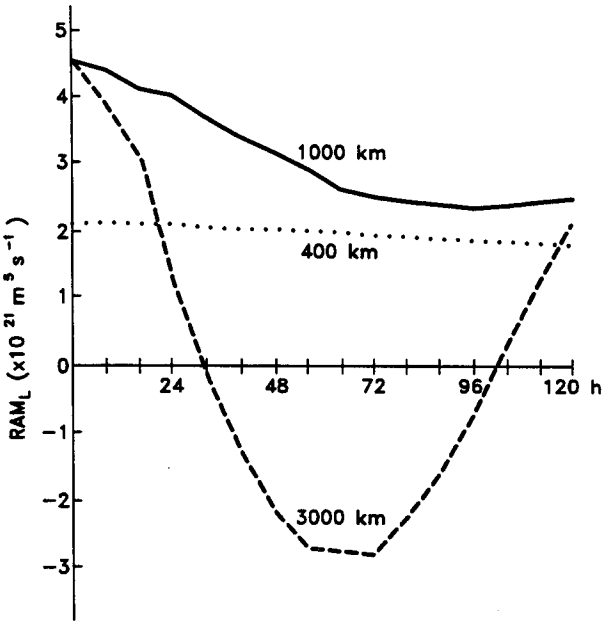

FIG. 7. Total RAM$_L$ for benchmark experiment, inside circles of radius 400, 1000 and 3000 km.

lates with the center of the vortex [the "Lagrangian" system; cf. Holland (1983)]. The wind relative to the moving center is designated by a subscript "L":

$$\mathbf{u}_L \equiv \mathbf{u} - \mathbf{c},$$

where $\mathbf{c} = (c_x, c_y)$ is the instantaneous velocity of the vortex center. The RAM in the moving coordinate system, designated RAM$_L$, is defined as in (3), but with relative tangential wind V_L. Thus,

$$\mathrm{RAM}_L = \iint (hrV_L)dA. \qquad (7)$$

Figure 7 shows the time dependence of total RAM$_L$ to 120 h, inside circles of radius 400, 1000 and 3000 km centered on the vortex. RAM$_L$ in $r \leqslant 400$ km decreases slightly. RAM$_L$ in $r \leqslant 1000$ km, the initial extent of the vortex, decreases by about 50% during the first 96 h, and then increases. For circles of radius greater than 1250 km RAM$_L$ crosses zero. In $r \leqslant 3000$ km, RAM$_L$ decreases rapidly and passes through zero at about 32 h; it reaches a minimum negative value at about 64 h, then increases to a positive value by 120 h. RAM$_L$ inside larger areas (not shown) is also characterized by a rapid decrease followed by an oscillation about zero. This oscillation is due to the development of successive anticyclonic and cyclonic gyres at larger and larger distances in the Rossby wave wake behind the vortex. The development of the primary anticyclonic gyre just to the east of the cyclone (see Fig. 2) induces an outer anticyclone in the azimuthally averaged tangential wind, as computed by Fiorino and Elsberry (1989a); this anticyclone is associated with the initial decrease in RAM$_L$.

The contributions to the changes in RAM$_L$ can be established with an angular momentum budget

$$\partial^L(\mathrm{RAM}_L)/\partial t = -\iint [hf(\mathbf{x} - \mathbf{x}_c)\cdot\mathbf{u}]dA - \oint (hrV_L\mathbf{u}_L\cdot\mathbf{n})ds, \quad (8)$$

where the area and boundary integrals refer to the circular area with specified radius. Here $\mathbf{x} - \mathbf{x}_c$ is the position vector with origin at the vortex center $\mathbf{x}_c$, and $\mathbf{n}$ is the outward unit normal vector. The time derivative $\partial^L(\ )/\partial t = \partial(\ )/\partial t + \mathbf{c}\cdot\nabla(\ )$ is the local change in the translating system [cf. Appendix 1 of Holland (1983)]. The first term on the right-hand side of (8) is the source of RAM$_L$ inside the circle due to the Coriolis torque, and the second is the inward flux of angular momentum across the circle. Note that the Coriolis torque is evaluated with the earth-based wind $\mathbf{u}$, and *not* the relative wind $\mathbf{u}_L$. There is no net pressure torque in (8) because the boundary is circular.

Figure 8 shows the Coriolis torque and angular momentum flux for circular areas with radius 1000 and 3000 km. The oscillation of RAM$_L$ over the large (3000 km) area (see Fig. 7) is dominated by the Coriolis torque. The gradual decrease of RAM$_L$ in $r \leqslant 400$ km (Fig. 7) is similarly controlled by the torque (not

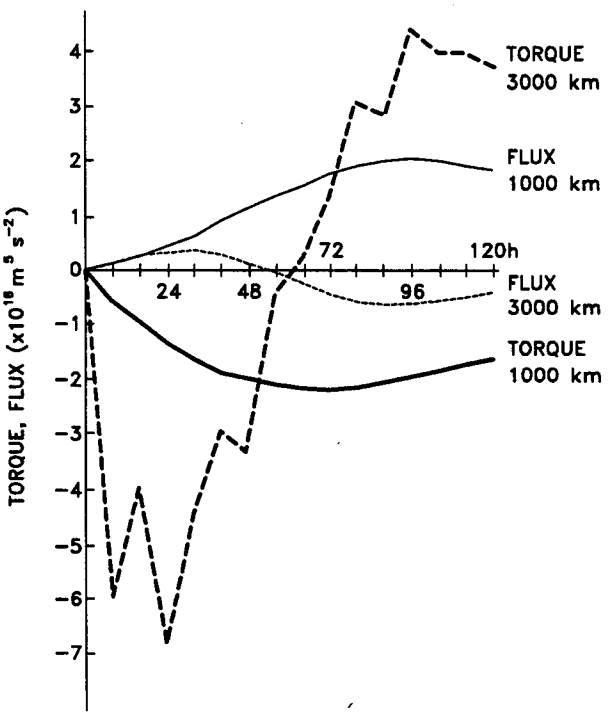

FIG. 8. Coriolis torque and angular momentum flux for benchmark experiment, inside circles of radius 1000 and 3000 km.

shown). In general the angular momentum flux tends to counteract the effect of the torque. For the circular area with radius 1000 km, in particular, there is a near balance between a net anticyclonic Coriolis torque and an inward angular momentum flux. The contributions to the balance are most clearly illustrated with the asymmetric wind, defined as the difference between the total wind ($\mathbf{u}$ or $\mathbf{u}_L$) and the symmetric wind about the vortex center ($\hat{\mathbf{u}}$ or, equivalently, $\hat{\mathbf{u}}_L$). The symmetric wind is derived by transforming the total wind into radial and tangential components, taking the azimuthal average of these components about the vortex center, and then transforming back to Cartesian coordinates.

The asymmetric wind in the benchmark experiment at 120 h is shown in Fig. 9 for the region within ~1000 km of the vortex center. Figure 9a shows the earth-based asymmetric wind, $\mathbf{u}' = \mathbf{u} - \hat{\mathbf{u}}$. The broad southeasterly flow between the cyclonic and anticyclonic gyres to the east and west of the vortex center advects the vortex to the northwest. This flow was also described by Fiorino and Elsberry (1989a). The overall southerly flow across the region produces an anticyclonic Coriolis torque to the north of the vortex center, and a cyclonic torque to the south. Since f is greater in the northern part of the domain, there is a net anticyclonic torque. Figure 9b shows the asymmetric wind in the vortex-centered coordinate system, $\mathbf{u}'_L = \mathbf{u}_L - \hat{\mathbf{u}}_L$. The relative wind is very nearly zero at the center of the vortex, which indicates that the center moves essentially with the total wind $\mathbf{u}$ (cf. Fiorino and Elsberry 1989a). The weak westerly flow across the vortex is connected to a southward flow in the northwest and southeast quadrants. The southward flow is cyclonic and inward in the northwest quadrant, and anticyclonic and outward in the southeast. The net angular momentum flux across the 1000 km circle centered on the vortex is therefore inward, counteracting the net anticyclonic Coriolis torque. The significance of the westerly flow across the vortex in the establishment of a near-steady state is discussed in section 5.

b. *Dependence on initial RAM*

The details of the evolution and motion of the vortex, including the establishment of a near-steady state, are determined by nonlinear processes. The relationship between the initial RAM and its future evolution is thus not a simple one. As seen above, once a vortex is no longer isolated the RAM within a circular area is different from that of the initial condition and, indeed, depends on the circle's radius. Thus, the assignment of a single value of RAM to "the vortex" is no longer possible.

The isolation theorem by Flierl et al. (1983) does, however, provide the context for studying vortices with different initial RAM. The remote effect due to the Rossby wave radiation field, at distances from the center large enough that the initial vortex can be approximated as a point source, will be proportional to the total initial RAM. If the initial RAM = 0, no remote radiation field is produced, and the vortex remains isolated. Figure 6b shows the wind at 120 h from a simulation using the initial vortex with RAM = 0 in Fig. 1. The remote influence of the vortex is negligible. An evaluation of RAM_L confirms that the vortex remains isolated, with $\mathrm{RAM}_L \approx 0$ within any circle larger than ~1000 km. For comparison, Fig. 6c shows the result of a simulation with an initial vortex identical to that with zero RAM, but without the outer anticyclone. That is, the tangential wind V is set equal to zero in the region $r \geq 600$ km, where $V < 0$ for the RAM = 0 vortex in Fig. 1. This initial vortex is cyclonic, but with total RAM = 1.7×10^{21} m^5 s^{-1}, which is ~0.35 times that of the benchmark vortex (RAM = 4.7×10^{21} m^5 s^{-1}) used in Fig. 6a. The shape of the remote radiation field in Fig. 6c is the same as that in Fig. 6a, but with a magnitude correspondingly two to three times smaller.

The motion of the vortex is not similarly related to its initial RAM. Figure 10 shows the tracks of the three vortices simulated in Fig. 6. At 120 h, the benchmark vortex has a velocity $\mathbf{c} = (-1.0, 1.6)$ m s^{-1}; the RAM = 0 vortex, $\mathbf{c} = (-0.3, 1.1)$ m s^{-1}; the vortex with intermediate initial RAM, $\mathbf{c} = (-0.3, 1.7)$ m s^{-1}. Each of the vortices moves on a large anticyclonic arc, apparently rotated this way by the initial or induced anticyclonic gyre seen in the azimuthal mean (see Fiorino and Elsberry 1989a). Clearly, neither the westward nor the northward speeds are proportional to the initial RAM. Such a proportionality was derived for the northward speed in Willoughby's (1988) linear analysis, and was implicit in Rossby's (1948) study. Most particularly, of course, the RAM = 0 vortex is not stationary. Moreover, the northward speed of the intermediate vortex is about the same as that of the benchmark vortex, even though the initial RAM of the latter is nearly three times as large.

c. *Discussion*

The results of this section confirm that use of an isolated initial symmetric hurricane vortex, with the total RAM constrained to be near zero, minimizes the remote, "far-field" influence due to Rossby wave adjustments. It was also found, however, that the motion of the vortex is not related to the initial RAM in any simple way. Vortex motion is determined by "near-field" Rossby wave dispersion. As discussed in section 4a, the vortex moves due to an interaction among many scales. Because the total RAM is an integral property of the vortex, an unlimited number of possible vortex profiles exist for a given RAM. The effect of a given modification to the outer structure of a barotropic vortex on its track cannot be predetermined from the initial RAM alone.

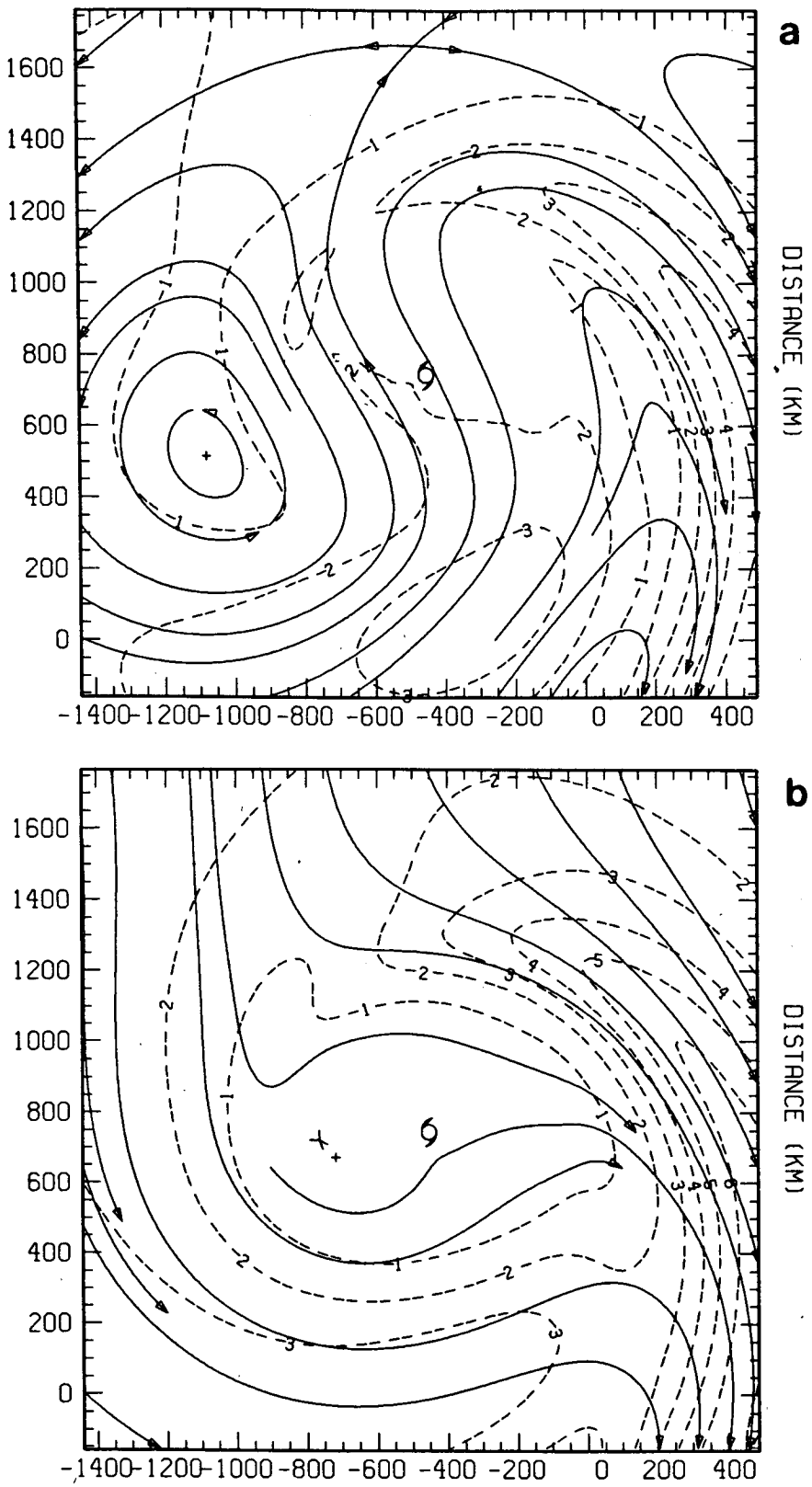

FIG. 9. Asymmetric wind in benchmark experiment at 120 h. Isotach interval is 1 m s^{-1}. (a) Earth-based wind, $\mathbf{u}'$; (b)wind in translating, vortex-centered coordinate system, $\mathbf{u}'_L$.

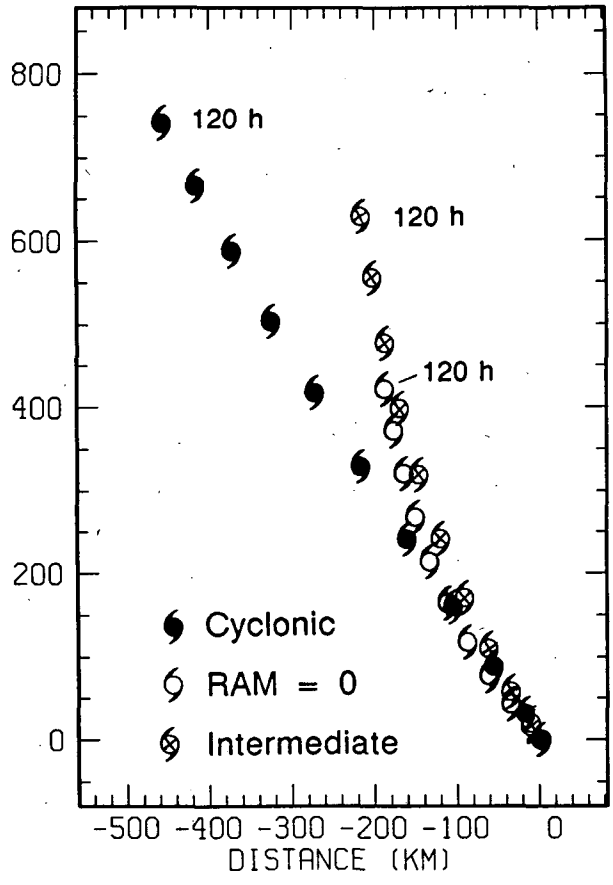

FIG. 10. Positions of vortex center every 12 h for vortex with initially cyclonic winds, total RAM = 0, and intermediate RAM.

The total RAM can be used, however, as a general guide when constructing a vortex profile. In the nondivergent situation, the remote influence of a nonisolated vortex extends to infinity. A term proportional to the streamfunction tendency can be added to the vorticity equation to simulate the inclusion of divergence in a quasi-geostrophic model (Cressman 1958). The use of a shallow water system, or the inclusion of the additional term in the vorticity equation, restricts the remote influence to distances from the vortex on the order of the Rossby radius. DeMaria (1987) made predictions of tropical cyclone tracks with a nondivergent barotropic model, including the additional streamfunction tendency term. In one set of experiments he evaluated the influence of the RAM of the initially symmetric vortex on mean forecast error (see Fig. 8 of DeMaria 1987). DeMaria (1987) found that the forecast error was minimum for an initial RAM that was not too far from zero. This result is consistent with the present discussion. Too large an initial RAM will lead too strong an interaction with the environment, or the model boundaries, and an incorrect forecast.

5. Near-steady state

Within a few days the near-vortex asymmetries approach a quasi-steady state. Fiorino and Elsberry (1989a) have found that the strength of the large-scale asymmetric gyres that advect the vortex to the northwest becomes approximately steady. They attribute this equilibration to a balance between linear Rossby dispersion, which generates the asymmetric gyres, and nonlinear advection by the symmetric wind, which rotates the gyres. As the near-steady state is approached, the speed and direction of vortex motion become approximately constant as well (Fig. 10; see also DeMaria 1985). The system evolves, and the vortex accelerates, but only slowly.

The asymmetric structure of the benchmark vortex in its near-steady state was shown in Fig. 9. The primary asymmetry is azimuthal wavenumber $n = 1$. The wavenumber one wind in the vortex-centered coordinate system, $\mathbf{u}'_L$ $(n = 1)$, is shown in Fig. 11a. The relative wind at the vortex center is only 0.3 m s^{-1}. Thus, as noted in section 4, the center moves essentially with the total wind. The westerly wind across the vortex, within ~350 km of the center, tends to blow around the center, parallel to the isotachs. Outside ~350 km the flow matches on to the environment, as described in the discussion of Fig. 9b above. The relative wind in the corresponding linear solution derived by Willoughby (1988; his Fig. 16e) is similarly weak and westerly across the vortex, also tending to deviate around the center.

The vorticity of the wind in Fig. 11a, designated ζ' $(n = 1)$, is shown in Fig. 11b. Relative vorticity extrema appear about 600 km from the center in the northeast and southwest quadrants. The region within 350 km of the center has a near-uniform southward relative vorticity gradient. Figure 11c shows the corresponding absolute vorticity, $\beta(y - y_c) + \zeta'$ $(n = 1)$. A region of nearly uniform absolute vorticity is evident out to the 350 km radius. In this region, therefore, $\nabla\zeta' \approx (0, -\beta)$; the relative vorticity gradient is nearly equal in magnitude but opposite in sign to that of the Coriolis parameter f.

The asymmetries in the inner region appear to be a universal feature, essentially independent of the initial vortex structure and direction of motion. A similar region of westerly relative wind with near-homogeneous asymmetric absolute vorticity (AAV) is seen in simulations with the RAM = 0 vortex, which moves in a more northerly direction than the benchmark experiment. Another simulation with a vortex with sufficiently strong anticyclone that its total RAM is the negative of the benchmark vortex moves to the south [results not shown]. This simulation develops a westerly flow across the vortex and a region of near-constant AAV as well.

The homogenization of AAV is not substantially influenced by vortex stretching. A simulation with the

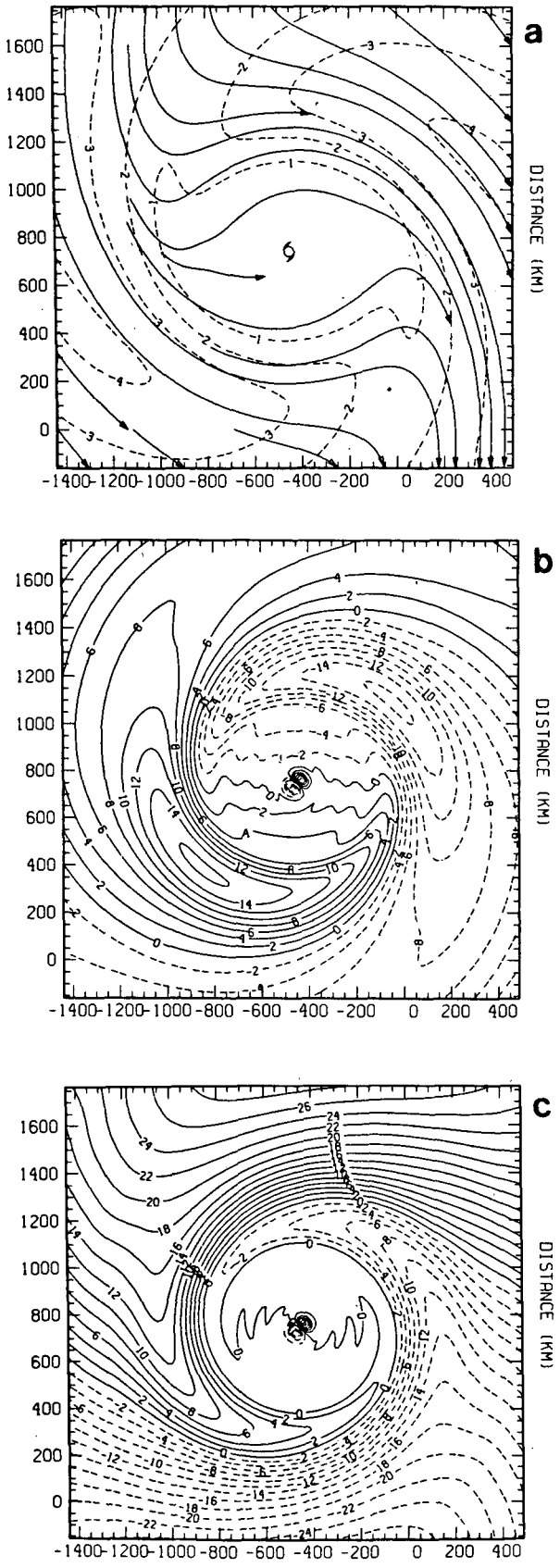

nondivergent model gives essentially the same structure as that in Fig. 11. The impact of the homogenization on the vortex evolution can thus be evaluated from the vorticity equation (4), with $\delta = 0$. The total wind is decomposed into its symmetric and relative components, plus the vortex motion: $\mathbf{u} = \hat{\mathbf{u}}_L + \mathbf{u}'_L + \mathbf{c}$. Correspondingly, $\zeta = \hat{\zeta} + \zeta'$. Then, from (4),

$$\partial^L(\hat{\zeta})/\partial t + \partial^L(\zeta')/\partial t + (\hat{\mathbf{u}}_L + \mathbf{u}'_L)\cdot\nabla\zeta' + \mathbf{u}'_L\cdot\nabla\hat{\zeta} + \beta(\hat{v}_L + v'_L + c_y) = 0. \quad (9)$$

As in (8), the time derivative is the local change in the translating, vortex-centered coordinate system. The term proportional to β is the linear dispersion due to planetary effects that generates the asymmetries (cf. Chan and Williams 1987; Fiorino and Elsberry 1989a). In the near-homogeneous region where $\nabla\zeta' \approx (0, -\beta)$,

$$(\hat{\mathbf{u}} + \mathbf{u}'_L)\cdot\nabla\zeta' \approx -\beta(\hat{v}_L + v'_L).$$

Then, (9) reduces to

$$\partial^L(\hat{\zeta})/\partial t + \partial^L(\zeta')/\partial t + \mathbf{u}'_L\cdot\nabla\hat{\zeta} + \beta c_y \approx 0. \quad (10)$$

The symmetric part of (10), $\partial^L(\hat{\zeta})/\partial t + \beta c_y \approx 0$, is a simple consequence of the conservation of angular momentum. When the vortex moves north, it spins down. The asymmetric part of (10), $\partial^L(\zeta')/\partial t + \mathbf{u}'_L\cdot\nabla\hat{\zeta} \approx 0$, represents the generation of asymmetries by the advection of symmetric vorticity by the relative asymmetric wind. As the westerly wind blows through the region, distortions of the vortex do occur. The major portion of the planetary term that established the asymmetries has, however, been cancelled by the asymmetric flow itself.

A likely mechanism for the homogenization of AAV in the present experiments can be inferred from recent studies by Carr and Williams (1989) and Smith (1989). These studies discuss the role of radial variations of angular velocity of the symmetric wind in creating small scales. In regions where $V(r)/r$ varies with radius, tangential advection of AAV by the symmetric wind will lead to progressively smaller scales. A fine-scale structure does appear in the absolute vorticity field computed from the total asymmetric wind in the present experiment (not shown). Although no explicit diffusion is included in the numerical model, the spectral transform by integration, in conjunction with the sixth-order filter (see section 2), removes energy at unrepresentable wavelengths. Thus, scales at the bottom of the enstrophy cascade are effectively removed. Homogenization of the fine-scale AAV then naturally occurs. Doubling the resolution in the benchmark experiment does not change the region of homogeneous AAV sub-

FIG. 11. Wavenumber 1 asymmetric component in benchmark experiment at 120 h. (a) Relative wind, $\mathbf{u}'_L$ ($n = 1$) [isotach interval 1 m s^{-1}]; (b) vorticity, ζ' ($n = 1$) [contour interval 2×10^{-6} s^{-1}]; (c) absolute vorticity, $\beta(y - y_c) + \zeta'$ ($n = 1$) (contour interval 2×10^{-6} s^{-1}).

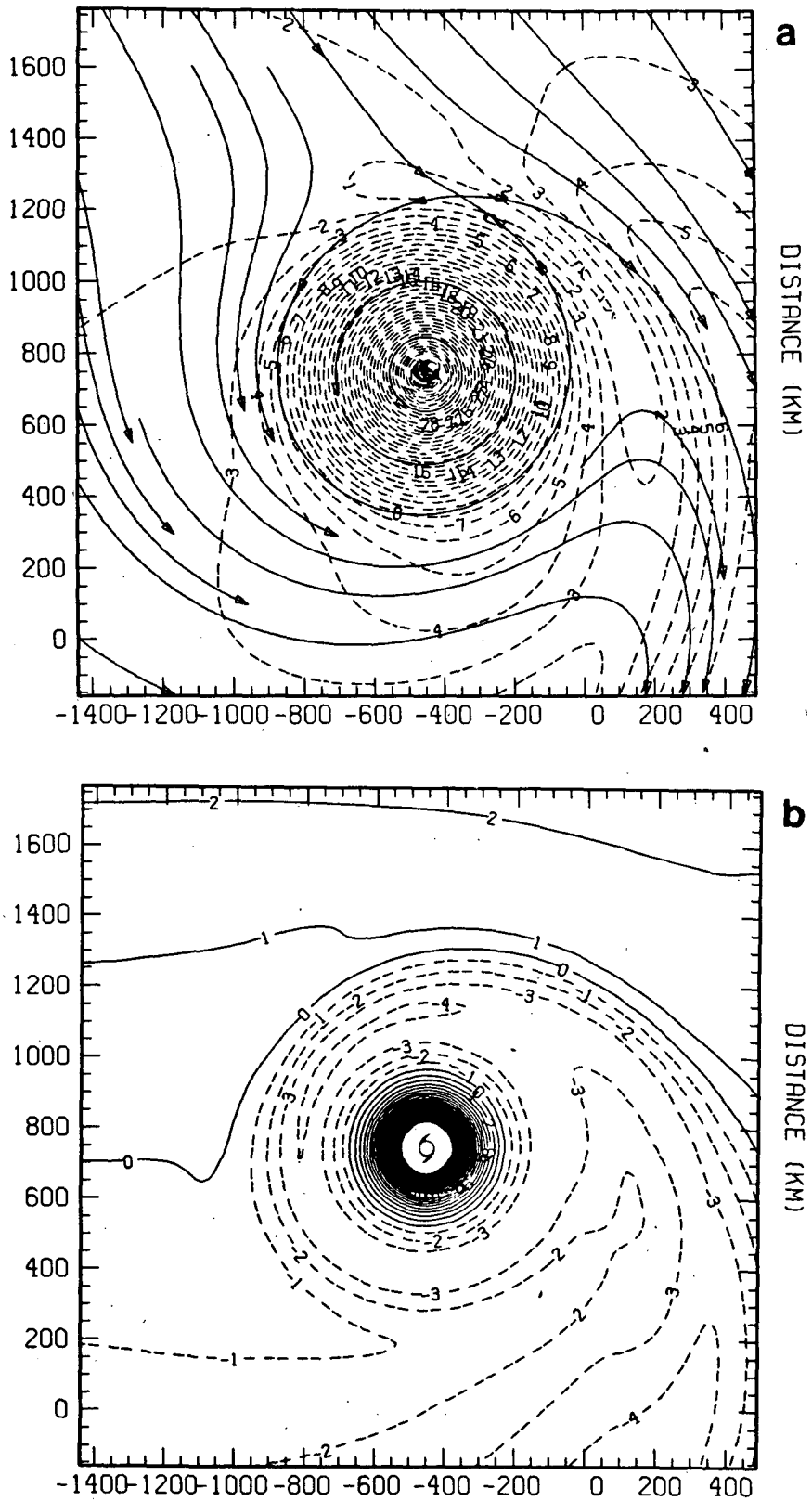

FIG. 12. Total solution in benchmark experiment at 120 h. (a) Relative wind, $\mathbf{u}_L$ [isotach interval 1 m s^{-1}]; (b) absolute vorticity, $\beta(y - y_c) + \zeta$ (contour interval 1×10^{-5} s^{-1}).

stantially. Thus, although removal of energy at the smallest scales is required for homogenization, the process is not controlled by the exact wavelengths that are removed.

The region over which the homogenization occurs can be characterized by the total fields. Figure 12a displays the total relative wind, $\mathbf{u}_L$, for the same situation as in Fig. 11; Fig. 12b shows the corresponding total absolute vorticity, $\beta(y - y_c) + \zeta$. The streamlines and total absolute vorticity contours within ~350 km of the vortex center are nearly circular, and therefore coincident. The homogenization of AAV seen in Fig. 11c occurs inside the vortex gyre, where both the streamlines and contours of total absolute vorticity are closed. As seen by the very small dipole in Fig. 11c, homogenization of the AAV does not occur in the vortex core. The vortex is in near solid-body rotation in $r < 40$ km. Since the angular velocity in the vortex core is then nearly independent of radius, the production of fine-scale structure does not occur. Induced asymmetries in the core simply rotate about the center.

6. Effect of environmental wind

The results of sections 4 and 5 have been extended to include an environmental wind with a meridional vorticity gradient. The background wind, $\bar{\mathbf{u}}$, is taken to be strictly zonal; $\bar{\mathbf{u}} = (\bar{u}, 0)$, where

$$\bar{u} = \bar{u}_0 \sin(ky), \tag{11}$$

with $\bar{u}_0 = 10$ m s^{-1} and $k = 2\pi/(3840$ km). The sinusoidal wavelength is chosen to give $\bar{u} = 0$ at the northern and southern boundaries of the domain. The vorticity associated with the background wind is

$$\bar{\zeta} = -(1.64 \times 10^{-5}\ \text{s}^{-1}) \cos(ky), \tag{12}$$

while the meridional vorticity gradient is

$$\bar{\zeta}_y = (2.68 \times 10^{-11}\ \text{m}^{-1}\ \text{s}^{-1}) \sin(ky). \tag{13}$$

The magnitude of the gradient is comparable to β. The background wind is initially in geostrophic balance with the height, taken to be

$$\bar{h} = (\bar{u}_0/g)[(f/k) \cos(ky) - (\beta/k^2) \sin(ky)]. \tag{14}$$

The background potential vorticity gradient due to the variation in $\bar{h}$ is much less than that due to $\bar{\zeta}$.

The domain and grid specifications are identical with those described in section 2. Instead of open boundaries, however, a channel model is used. The domain is cyclic east–west. On the northern and southern boundaries $\mathbf{u} = 0$ and $h_{yy} = -k^2 h$ are specified. The background wind and height are, by themselves, a stable, steady state solution to the equations of motion (1) and (2).

For the simulations described in the present section, an initial symmetric vortex is added to the background wind and height. Figure 13 displays the tracks of the initial cyclonic and RAM = 0 vortices shown in Fig. 1. As the vortex moves northward, it first encounters a westerly environmental wind with a positive vorticity gradient. As inferred by Kasahara and Platzman (1963), and verified by DeMaria (1985), the positive vorticity gradient accelerates the vortex more to the north than does the beta effect alone. Up to 72 h the vortices in Fig. 13 each move to the north more rapidly than did the corresponding vortex without an environmental flow (Fig. 10). As was also the case with no background wind, the RAM = 0 vortex moves more slowly to the north than does its cyclonic counterpart. After 72 h, however, the complex interaction between the vortices and the environmental wind alters the tracks. The northward motion of each vortex decelerates, and turns toward the south by 120 h near the latitude of zero background vorticity and maximum of $\bar{\zeta}_y$. This result contradicts those of Kasahara and Platzman (1963) and DeMaria (1985), who obtain a northward motion where $\bar{\zeta}_y > 0$.

Even in the presence of the environmental vorticity gradient, the near-vortex wind evolves to a state very similar to that described in section 5. Figure 14 displays the relative wind for the cyclonic vortex at 120 h. The asymmetric wind $\mathbf{u}'_L$, shown in Fig. 14a, has a significant azimuthal wavenumber 2 component. The westerly wind across the vortex, characteristic of the near-steady state described in section 5, is seen more clearly in the wavenumber 1 component $\mathbf{u}'_L$ ($n = 1$) shown in Fig. 14b. As with the vortex in the quiescent environment (Fig. 11a), the relative wind at the center is nearly calm. The vortex center moves with the total wind.

Figure 15 shows the AAV corresponding to the wind in Fig. 14. The wavenumber 1 component in Fig. 15b displays a region of near-uniform AAV near the vortex center, just as in the resting environment (Fig. 11c). The magnitude of the absolute vorticity gradient $\beta + \bar{\zeta}_y$ near the vortex center is about twice β. The uniformity of the wavenumber one AAV in Fig. 15b within 300 km of the vortex center thus indicates a very effective homogenization. The total effective beta is neu-

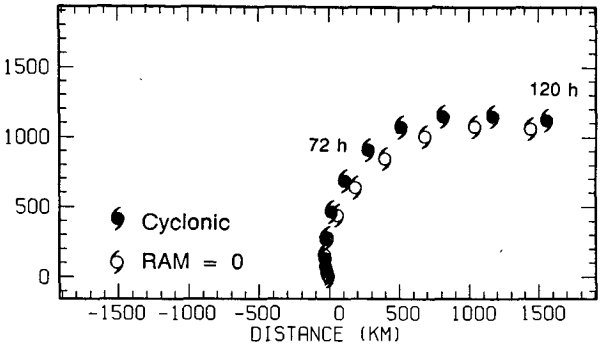

FIG. 13. Positions of vortex center every 12 h in sinusoidal zonal background flow, $\bar{\mathbf{u}}$. For vortex with initially cyclonic winds, and total RAM = 0.

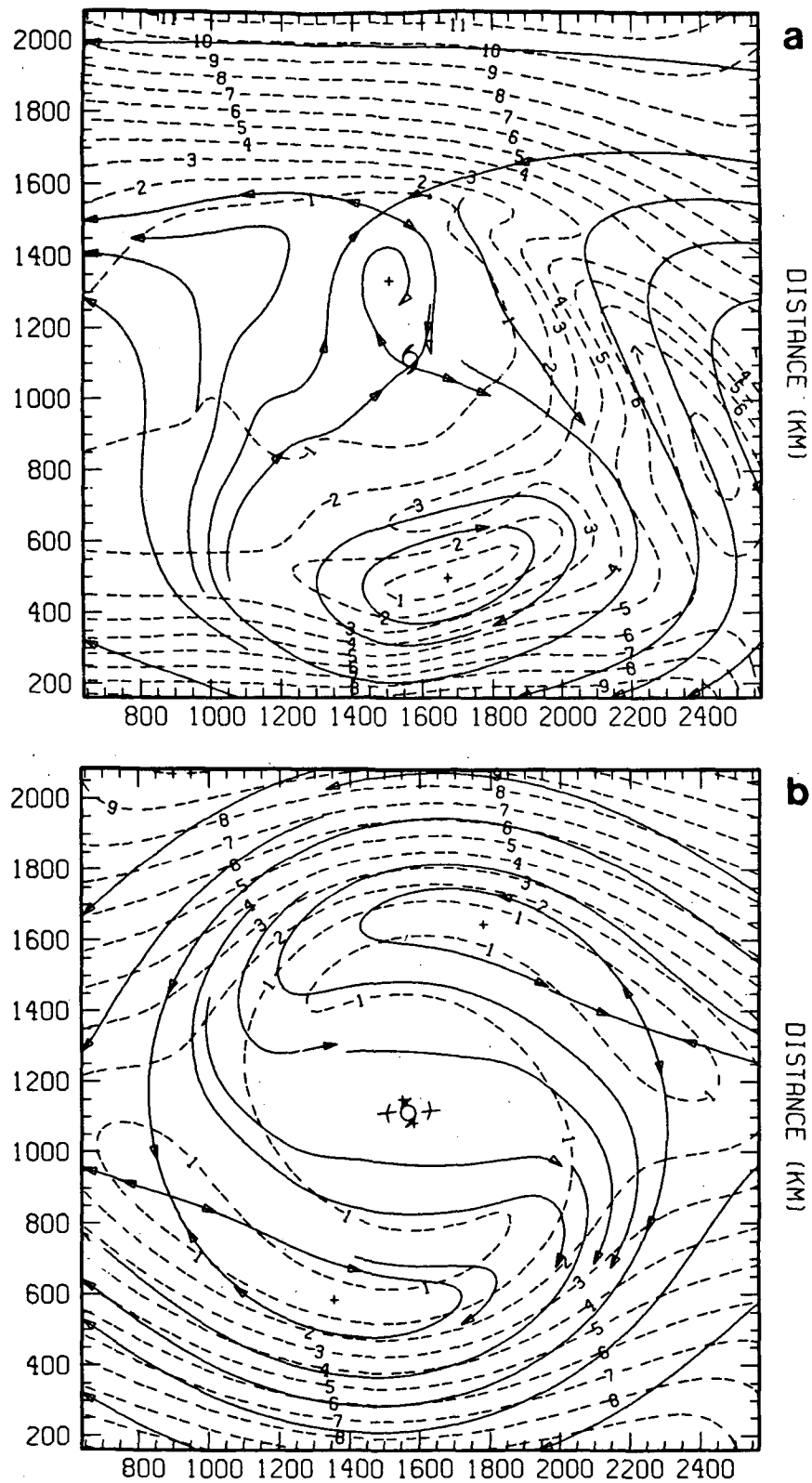

FIG. 14. Relative wind at 120 h for initially cyclonic vortex in background zonal flow. Isotach interval is 1 m s^{-1}. (a) Asymmetric wind, $\mathbf{u}'_L$; (b) wavenumber 1 component, $\mathbf{u}'_L$ ($n = 1$).

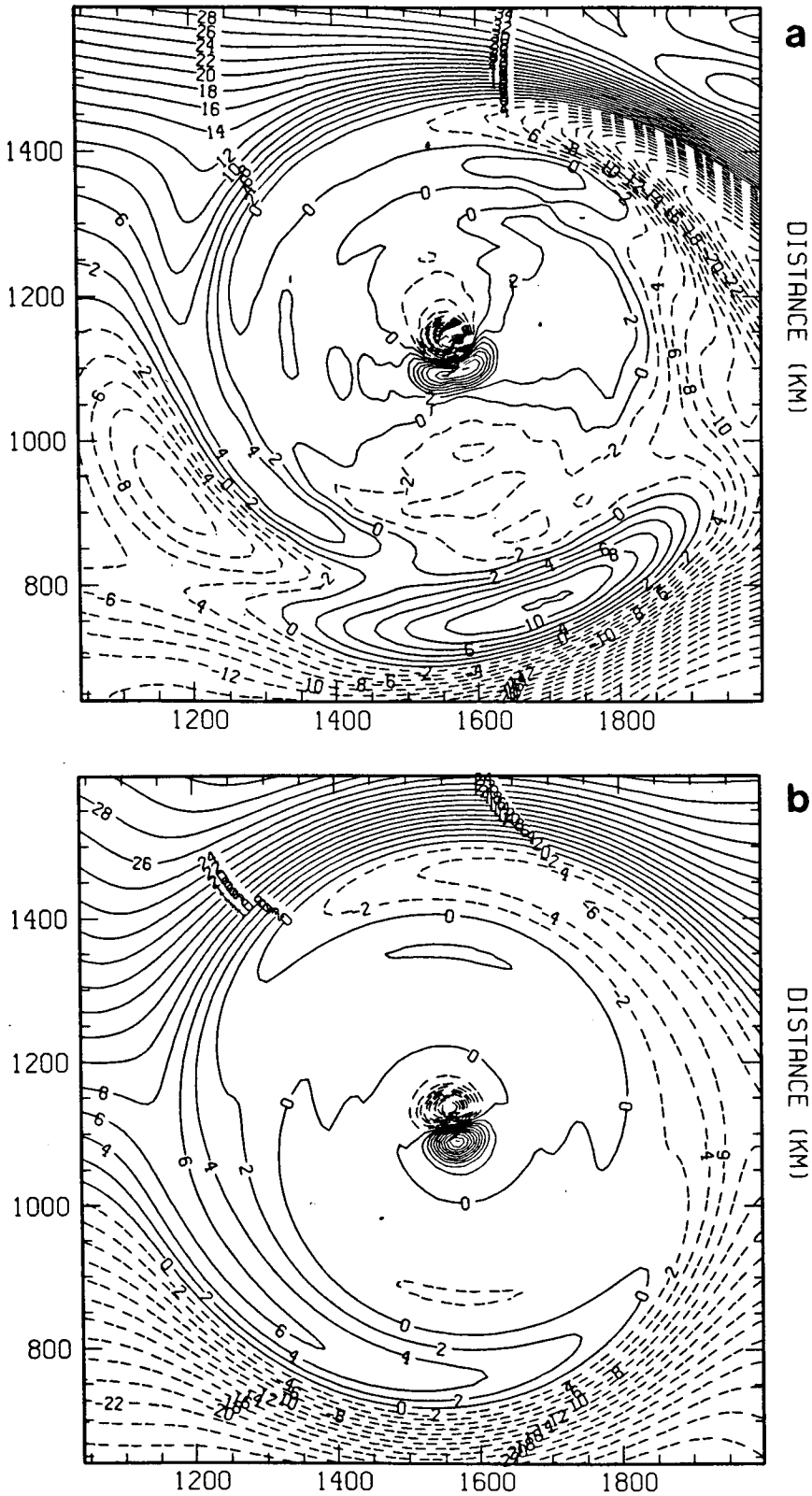

FIG. 15. Absolute vorticity at 120 h for initially cyclonic vortex in background flow. Contour interval is 2×10^{-6} s^{-1}. (a) Asymmetric absolute vorticity, $\beta(y - y_c) + \zeta'$; (b) wavenumber 1 component $\beta(y - y_c) + \zeta'$ $(n = 1)$.

tralized by the induced wavenumber 1 asymmetries. Induced asymmetries with wavenumber $n > 1$, however, produce a nonuniform AAV. The wavenumber 2 component of AAV, seen in Fig. 15a, is not homogenized. Wavenumber 2 asymmetries are generated by an interaction between the vortex and the shearing environmental current (Willoughby 1979). Although these higher wavenumber asymmetries near the vortex center are more rapidly homogenized than $n = 1$ (Carr and Williams 1989), the changing environmental conditions apparently create $n = 2$ asymmetries more rapidly than the shearing tangential wind destroys them. As in the resting environment, the wavenumber 1 AAV is homogeneous inside the vortex-dominated gyre, where the streamlines and contours of total absolute vorticity (not shown) are closed.

7. Discussion: generalization to 3-D

The results of this study were derived from simulations with a barotropic model. Divergence was found to have a very small effect on vortex motion, even for a shallow water depth of only 1 km (section 3). The situation is more complicated for a three-dimensional tropical cyclone forecast model. The observational results of Chan (1984), and more recent results from analyses using Omega dropwindsondes (J. Franklin, personal communication, 1989), imply that divergence may make a significant contribution to relative vorticity tendencies in the low or high troposphere. Divergence may thus be of some importance to vortex motion in a multilevel model.

Vertical shear will also complicate the evolution of RAM evaluated in section 4. The total RAM is determined in general not only by the radial profile, but also by the vertical structure of the vortex. An upper-level anticyclone will reduce the RAM from that of a low-level cyclone alone. In the absence of boundary stresses, the isolation theorem of Flierl et al. (1983) will still be valid. A surface drag will, however, tend to spin down the vortex. Such a boundary contribution to the integrated momentum balance invalidates the theorem; an initially isolated vortex, then, need not remain isolated. In the barotropic situation described in section 4, the Rossby wave adjustment process tended to reduce the RAM within a 1000 km radius circle. It remains to be determined whether a similar adjustment process will tend to counteract the vortex spin-down due to surface drag.

Either external or internal forcing may also alter the homogenization of AAV in the closed vortex gyre. When thickness changes due to divergence are significant, potential vorticity rather than absolute vorticity will tend to be homogenized. Rhines and Young (1982) presented a theory designed to explain the tendency for the homogenization of the total potential vorticity in planetary gyres, when such forcing is small. The potential vorticity in Rhines and Young's (1982) analysis mixes by a down-gradient eddy flux across the closed time-mean isolines. The mixing of the AAV in the present experiments, on the other hand, is likely accomplished by the radial shear of the symmetric circulation. Homogenization in the present study, as in Rhines and Young (1982), requires removal of energy at the smallest scales. In the presence of external forcing, such as surface friction, or internal heating, the ability to create a homogeneous region of AAV may be altered. The strong tendency for homogenization seen in the present study does, however, confirm its importance in maintaining the integrity of the barotropic vortex in the presence of dispersive influences. The neutralization of the beta effect by the asymmetries "isolates" the vortex, allowing it to move relatively undistorted by environmental influences. Research is in progress to evaluate the extension of the present results to a three-dimensional model.

Acknowledgments. Discussions with Drs. Mark DeMaria and Hugh Willoughby during the course of this research, and their comments on an earlier version of this paper, have helped clarify both thought and presentation. Dr. DeMaria implemented the nondivergent model used in section 3.

REFERENCES

Anthes, R. A., and J. E. Hoke, 1975: The effect of horizontal divergence and the latitudinal variation of the Coriolis parameter on the drift of a model hurricane. *Mon. Wea. Rev.*, **103**, 757–763.

Carr, L. E., and R. T. Williams, 1989: Barotropic vortex stability to perturbations from axisymmetry. *J. Atmos. Sci.*, **46**, 3177–3191.

Chan, J. C.-L., 1984: An observational study of the physical processes responsible for tropical cyclone motion. *J. Atmos. Sci.*, **41**, 1036–1048.

——, and R. T. Williams, 1987: Analytical and numerical studies of the beta-effect in tropical cyclone motion. Part I: Zero mean flow. *J. Atmos. Sci.*, **44**, 1257–1265.

Cressman, G. P., 1958: Barotropic divergence and very long atmospheric waves. *Mon. Wea. Rev.*, **86**, 293–297.

DeMaria, M., 1985: Tropical cyclone motion in a nondivergent barotropic model. *Mon. Wea. Rev.*, **113**, 1199–1210.

——, 1987: Tropical cyclone track prediction with a barotropic spectral model. *Mon. Wea. Rev.*, **115**, 2346–2357.

Fiorino, M., and R. L. Elsberry, 1989a: Some aspects of vortex structure related to tropical cyclone motion. *J. Atmos. Sci.*, **46**, 975–990.

——, and ——, 1989b: Contributions to tropical cyclone motion by small, medium and large scales in the initial vortex. *Mon. Wea. Rev.*, **117**, 721–727.

Flierl, G. R., 1977: The application of linear quasi-geostrophic dynamics to Gulf Stream rings. *J. Phys. Oceanogr.*, **7**, 365–379.

——, M. E. Stern and J. A. Whitehead, Jr., 1983: The physical significance of modons: Laboratory experiments and general integral constraints. *Dyn. Atmos. Oceans*, **7**, 233–263.

Gill, A. E., 1980: Some simple solutions for heat-induced tropical circulation. *Quart. J. Roy. Meteor. Soc.*, **106**, 447–462.

Goldenberg, S. B., S. D. Aberson and R. E. Kohler, 1987: An updated, fine-grid version of the operational barotropic hurricane-track prediction model. *Extended Abstracts: 17th Conference on Hurricanes and Tropical Meteorology*, Boston, Amer. Meteor. Soc., 86–89.

Holland, G. J., 1983: Angular momentum transports in tropical cyclones. *Quart. J. Roy. Meteor. Soc.*, **109**, 187–209.

Kasahara, A., and G. W. Platzman, 1963: Interaction of a hurricane with the steering flow and its effect upon the hurricane trajectory. *Tellus,* **15,** 321–335.

Kitade, T., 1981: A numerical study of the vortex motion with barotropic models. *J. Meteor. Soc. Japan,* **59,** 801–807.

Lim, H., and C.-P. Chang, 1983: Dynamics of teleconnections and Walker circulations forced by equatorial heating. *J. Atmos. Sci.,* **40,** 1897–1915.

Lindzen, R. S., 1967: Planetary waves on beta-planes. *Mon. Wea. Rev.,* **96,** 441–451.

——, and S. Nigam, 1987: On the role of sea surface temperature gradients in forcing low-level winds and convergence in the tropics. *J. Atmos. Sci.,* **44,** 2418–2436.

McWilliams, J. C., and G. R. Flierl, 1979: On the evolution of isolated, nonlinear vortices. *J. Phys. Oceanogr.,* **9,** 1155–1182.

——, P. R. Gent and N. J. Norton, 1986: The evolution of balanced, low-mode vortices on the β-plane. *J. Phys. Oceanogr.,* **16,** 838–855.

Neumann, C. J., and J. M. Pelissier, 1981: Models for the prediction of tropical cyclone motion over the North Atlantic: An operational evaluation. *Mon. Wea. Rev.,* **109,** 522–538.

Ooyama, K. V., 1984: A model for hurricane prediction. *Postprint Volume: 15th Conference on Hurricanes and Tropical Meteorology,* Boston, Amer. Meteor. Soc., 344–349.

——, 1987: Scale-controlled objective analysis. *Mon. Wea. Rev.,* **115,** 2479–2506.

Rhines, P. B., and W. R. Young, 1982: Homogenization of potential vorticity in planetary gyres. *J. Fluid. Mech.,* **122,** 347–367.

Rossby, C. G., 1948: On the displacement and intensity change of atmospheric vortices. *J. Mar. Res.,* **7,** 175–187.

Smith, R. K., W. Ulrich and G. Dietachmayer, 1989: A numerical study of tropical cyclone motion using a barotropic model. Part I. The role of vortex asymmetries. *Quart. J. Roy. Meteor. Soc.,* **116,** in press.

Willoughby, H. E., 1979: Excitation of spiral bands in hurricanes by interaction between the symmetric mean vortex and a shearing environmental steering current. *J. Atmos. Sci.,* **36,** 1226–1235.

——, 1988: Linear motion of a shallow-water, barotropic vortex. *J. Atmos. Sci.,* **45,** 1906–1928.

——, 1989: Gradient balance in tropical cyclones. *J. Atmos. Sci.,* in press.

Zangvil, A., 1977: On the presentation and interpretation of spectra of large-scale disturbances. *Mon. Wea. Rev.,* **105,** 1469–1472.